

RESEARCH ARTICLE | SEPTEMBER 20 2022

A non-equilibrium slip wall model for large-eddy simulation with an immersed boundary method

Beiji Shi (时北极) ✉; Zhaoyue Xu (许昭越); Shizhao Wang (王士召) ✉



AIP Advances 12, 095014 (2022)

<https://doi.org/10.1063/5.0101010>
View
OnlineExport
Citation

CrossMark

Articles You May Be Interested In

The response of plates to TBL excitation: High versus low wavenumber effects

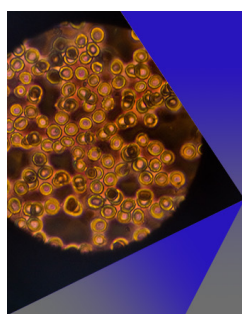
J Acoust Soc Am (August 2005)

Planar turbulent boundary layer (TBL) pressure field emulation with a reduced degree of freedom array

J Acoust Soc Am (August 2005)

Investigations of roughness-generated TBL sound using coupled physical-computational experiments in conjunction with theoretical development

J Acoust Soc Am (May 2008)



AIP Advances

Special Topic: Medical Applications
of Nanoscience and Nanotechnology

Submit Today!

A non-equilibrium slip wall model for large-eddy simulation with an immersed boundary method

Cite as: AIP Advances 12, 095014 (2022); doi: 10.1063/5.0101010

Submitted: 28 May 2022 • Accepted: 21 July 2022 •

Published Online: 20 September 2022




View Online



Export Citation



CrossMark

Beiji Shi (时北极),^{1,2} Zhaoyue Xu (许昭越),^{1,2} and Shizhao Wang (王士召)^{1,2,a)} 

AFFILIATIONS

¹ LNM, Institute of Mechanics, Chinese Academy of Sciences, Beijing 100190, China

² School of Engineering Sciences, University of Chinese Academy of Sciences, Beijing 100049, China

^{a)} Author to whom correspondence should be addressed: wangsz@lnm.imech.ac.cn

ABSTRACT

A non-equilibrium wall model for large-eddy simulation with the immersed boundary (IB) method is proposed to reduce the required number of grid points in simulating wall-bounded turbulence. The proposed wall model is presented as an appropriate slip velocity on the wall. The slip velocity is constructed by integrating the simplified turbulent boundary layer (TBL) equation along the wall-normal direction, which enhances the integral momentum balance near the wall on a coarse grid. The effect of pressure gradient on the near wall flow is taken into account by retaining the pressure gradient term in the simplified TBL equation. The proposed model is implemented in the form of a direct-forcing IB method with moving-least-square reconstruction near the wall. The benchmarks of plane channel turbulence and the flows over a backward-facing step are used for validation. The proposed model improves the wall stresses and velocity profiles in the region where the pressure gradient dominates the near wall flows.

© 2022 Author(s). All article content, except where otherwise noted, is licensed under a Creative Commons Attribution (CC BY) license (<http://creativecommons.org/licenses/by/4.0/>). <https://doi.org/10.1063/5.0101010>

I. INTRODUCTION

The purpose of this work is to develop a wall model within the framework of the immersed boundary (IB) method for the large-eddy simulation (LES) of turbulent flows. The wall models use approximate boundary conditions to circumvent excessive resolution of the flow near the wall and to avoid the prohibitive grid requirement for LES of wall-bounded turbulence at high Reynolds numbers.^{1–3} The IB method has advantages in handling flows with complex geometries and/or moving boundaries.^{4,5} The combination of wall models with the IB method is expected to provide a feasible tool for LES of turbulent flows with non-canonical walls.^{6–8}

The most widely used wall model is the wall stress model, which skips the flow details near the wall by modeling the inner-region of the turbulent boundary layer and feeds the LES with the wall stress boundary condition. Schumann⁹ proposed a wall stress model based on the logarithmic law of the wall to simulate the turbulent flows in plane channels and annuli. The model based on the logarithmic law of the wall can be constructed from the Reynolds-averaged

boundary layer equation by discarding the pressure gradient and convective terms, which is often referred to as the equilibrium wall model since the equilibrium stress balance.¹⁰ Correspondingly, the model based on the Reynolds-averaged boundary layer equation with pressure gradient and/or convective terms are often referred to as the non-equilibrium wall model. The equilibrium wall stress model was then improved by using the power-law velocity profiles to avoid numerically solving the non-linear equation,¹¹ accounting for the time shifting caused by the sweeps and ejections near the wall,¹² or including the effect of a buffer layer.¹³ John-Puthenveetil and Jakirlić¹⁴ proposed an adaptive wall model by referring to a universal expression for the near wall velocity profiles, where a parameter can be used to represent the non-equilibrium effect. Another way to account for the non-equilibrium effects is to use the two-layer model proposed by Balaras *et al.*¹⁵ in which the turbulent boundary layer (TBL) equation on an embedded mesh near the wall is solved. The non-equilibrium model is reported to give improved results compared with the equilibrium models for square duct and rotating channel flows. Recently, Yang *et al.*¹⁶ proposed an integral

wall model by adopting the classical integral method of von Kármán and Pohlhausen to avoid solving the differential TBL equation on an embedded mesh. Suga *et al.*¹⁷ further simplified the subgrid eddy viscosity to analytically integrate the boundary layer equation near the wall and obtained an algebraic non-equilibrium wall model. Cai and Sagaut¹⁸ proposed another algebraic wall model by expanding the near wall velocity profiles. Hosseinzadea and Bergstrom¹⁹ found that the performance of the wall model is affected by the temporal-filtering. A temporal-filtering period comparable to the turbulent diffusion timescale helps in removing the nonessential high-frequency wavelengths that disturb the inputs of the wall model. Wang *et al.*²⁰ proposed a method to generate synthetic flow fields based on a minimum flow unit, which provides an effective approach to constructing off-wall boundary conditions for wall-modeled LES. The details of the progress on the wall models for LES can be found in the review papers of Piomelli and Balaras,¹ Larsson *et al.*,²¹ and Bose and Park.²

To date, most of wall models are developed in the framework of the boundary conformal mesh method. The non-boundary conformal mesh method has attracted increasing attention in the last two decades for its simplicity in mesh generation and advantages in parallel computing.^{22–24} The combination of the wall models with the non-boundary conformal mesh method is expected to help in enhancing the LES of turbulent flows with complex geometries in engineering.^{25–27} However, the application of wall models to the non-boundary conformal mesh method is not straightforward due to the difficulties in correctly imposing a momentum flux on the boundaries with the non-boundary conformal mesh.^{28,29}

The IB method is a typical non-boundary conformal mesh method, in which the equations for fluid dynamics are usually solved on an Eulerian (Cartesian) mesh and the equations for solid or structural dynamics are usually solved on a Lagrangian mesh. The effects of solid boundaries on the flow are represented by body forces in the momentum equation for fluid dynamics.^{30–35} The computation of the body forces couples the variables on the Eulerian and Lagrangian meshes. The IB method has been successfully used in simulations of laminar flows with complex geometries and moving boundaries.^{36–41} However, the simulations of the turbulent flows by using the IB method are reported in only a few works.^{42–45} The application of the IB method to the high Reynolds number turbulent flows is of great challenge, mainly because of the difficulties in fully resolving the flows near the wall.^{7,46,47}

Tessicini *et al.*⁴⁸ introduced a wall model to the IB method to extend its capability to LES of turbulent flows. They solved the flow equations for LES to the second off-wall grid points and reconstructed the velocity on the off-wall grid points by solving the simplified TBL equations. The wall model significantly reduces the computational cost and notably improves the results compared to simulations without the wall model on the same grid. Instead of solving the simplified TBL equations, Choi *et al.*⁴⁹ reconstructed the velocity at the Eulerian grid points near the wall using the power law velocity profiles with high-order corrections. In addition to reconstructing the velocity at the Eulerian grid points near the wall, Roman *et al.*²⁸ suggested imposing a RANS-like eddy viscosity near the wall to preserve the balance between the driving force and the wall stress. Most of the wall models in the framework of the IB method are equilibrium wall models. A non-equilibrium wall model in conjunction with the IB method

is needed to take the advantages of the IB method in handling complex boundaries.

We propose a non-equilibrium wall model for LES with the IB method. The non-equilibrium wall model is imposed as a slip velocity on the wall. The slip velocity along the wall-parallel direction together with the transpiration velocity along the wall-normal direction has been reported to give an improved prediction of the turbulence intensities in the recent work of Bae *et al.*,^{50,51} in which the slip and transpiration velocities are obtained based on a differential filter. Yang and Bose⁵² showed that the slip wall model based on the differential filter is compatible with arbitrary LES filter and can be motivated using the RANS-type momentum equation. Therefore, we construct the slip-velocity based on an integral momentum equation near the wall, instead of using the differential filter. The proposed model is able to take into account the effects of pressure gradient. The benchmark flows of the plane channel turbulence and the flows over a backward-facing step are simulated to validate the proposed model.

This paper is organized as follows: In Sec. II, we briefly outline the governing equations and numerical method for LES. In Sec. III, we give the details of the proposed slip-wall model in the framework of the IB method. The validation and application of the model for canonical flows are presented in Sec. IV. Finally, the summary and conclusions are given in Sec. V.

II. GOVERNING EQUATIONS AND NUMERICAL METHOD FOR LARGE-EDDY SIMULATION

The governing equations for the LES of incompressible flow are the filtered continuity and Navier–Stokes equations

$$\frac{\partial \tilde{u}_i}{\partial x_i} = 0, \quad (1)$$

$$\frac{\partial \tilde{u}_i}{\partial t} + \frac{\partial \tilde{u}_i \tilde{u}_j}{\partial x_j} = -\frac{1}{\rho} \frac{\partial \tilde{p}}{\partial x_i} + \nu \frac{\partial^2 \tilde{u}_i}{\partial x_j \partial x_j} + \frac{\partial \tau_{ij}}{\partial x_j} + f_i, \quad (2)$$

where \tilde{u}_i ($i = 1, 2, 3$) and \tilde{p} are the filtered velocity and pressure, respectively, f_i ($i = 1, 2, 3$) is the body force that represents the boundary effect on the flow in the IB method, and ν and ρ are the kinematic viscosity and density of the fluid, respectively. The subgrid stress τ_{ij} is computed as

$$\tau_{ij} - \frac{1}{3} \tau_{kk} \delta_{ij} = 2\nu_{\text{SGS}} \tilde{S}_{ij}, \quad (3)$$

where \tilde{S}_{ij} is the resolved strain rate tensor. The subgrid scale (SGS) eddy viscosity ν_{SGS} is determined by the wall-adapting local eddy viscosity (WALE) model,⁵³ which is specifically designed to obtain the proper y^3 near-wall scaling for the eddy viscosity without requiring a dynamic procedure,

$$\nu_{\text{SGS}} = C_w^2 \tilde{\Delta}^2 \frac{(\mathcal{S}_{ij}^d \mathcal{S}_{ij}^d)^{3/2}}{(\tilde{S}_{ij} \tilde{S}_{ij})^{5/2} + (\mathcal{S}_{ij}^d \mathcal{S}_{ij}^d)^{5/4}}, \quad (4)$$

where

$$\mathcal{S}_{ij}^d = \frac{1}{2} (\tilde{g}_{ij}^2 + \tilde{g}_{ji}^2) - \frac{1}{3} \delta_{ij} \tilde{g}_{kk}^2 \quad (5)$$

is the traceless symmetric part of the tensor $\tilde{g}_{ij}^2 = \tilde{g}_{ik}\tilde{g}_{kj}$, with $\tilde{g}_{ij} = \partial\tilde{u}_i/\partial x_j$ being the resolved velocity gradient tensor. The constant parameter is set to $C_w = 0.6$. $\tilde{\Delta}$ is the subgrid characteristic length scale, which is taken as the grid length in this work.

The governing Eqs. (1) and (2) are numerically solved by using the projection method in combination with the IB method,⁴⁷

$$\frac{\tilde{u}_i^* - \tilde{u}_i^n}{\Delta t} = \text{rhs}^{n+1/2} - \frac{\partial \tilde{p}^n}{\partial x_i} + f_i^{n+1/2}, \tag{6}$$

$$\tilde{u}_i^{n+1} = \tilde{u}_i^* - \Delta t \frac{\partial \delta p}{\partial x_i}, \tag{7}$$

$$\frac{\partial^2 \delta p}{\partial x_i \partial x_i} = \frac{1}{\Delta t} \frac{\partial \tilde{u}_i^*}{\partial x_i}, \tag{8}$$

$$\tilde{p}^{n+1} = \tilde{p}^n + \delta p, \tag{9}$$

where the superscript n denotes the number of time step, \tilde{u}_i^* is the intermediate velocity, rhs represents the discretized advective and diffusive terms as well as the SGS stresses, Δt is the time step, and δp is the pressure correction. The second-order central difference scheme on a staggered Cartesian grid is used for the spatial discretization, and the second-order Adams–Bashforth method is used for time advancement. The body forcing f_i in the momentum equation represents the effects of immersed boundaries on the flow and will be discussed in Sec. III. The details of the numerical method can be found in Refs. 47 and 54. The validations and applications of the flow solver for a variety of flows can be found in Refs. 55–57.

III. SLIP WALL MODEL FOR LARGE-EDDY SIMULATION WITH THE IMMERSSED BOUNDARY METHOD

We report the construction and implementation of the proposed slip wall model in this section. The construction of the wall model is based on the integral momentum equation near the wall. The implementation of the slip wall model is based on the moving-least-square (MLS) direct-forcing IB method.⁵⁴ The details of the procedures are reported as follows.

A. Construction of the slip wall model

We construct the slip wall model in a local orthogonal coordinate system $o-\xi\eta\zeta$ as shown in Fig. 1. For a point W on the wall, the $o-\eta$ axis is along the wall-normal direction, the $o-\xi$ axis is parallel to the tangential velocity near the wall, and the $o-\zeta$ axis is perpendicular to the $o-\eta$ and $o-\xi$ axes according to the right-hand rule. The velocity near the wall can be decomposed as follows:

$$\vec{u} - \vec{u}_w \equiv \Delta \vec{u} = u_\eta \vec{e}_\eta + u_\xi \vec{e}_\xi, \tag{10}$$

where \vec{u}_w is the velocity at point W on the wall, \vec{e}_η and \vec{e}_ξ are the unit vectors in the wall-normal and tangential directions, respectively, and u_η and u_ξ are the normal and tangential components of the velocity in the local coordinate system $o-\xi\eta\zeta$, respectively. In the

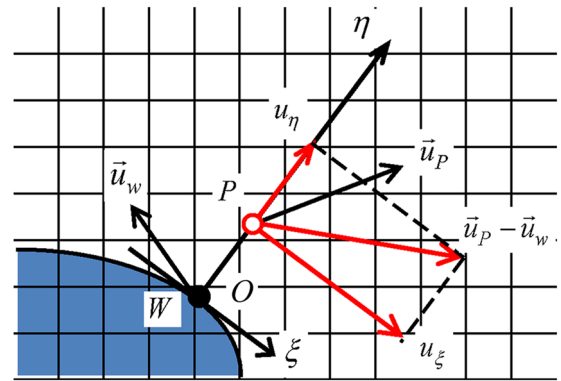


FIG. 1. Schematic illustration of the local orthogonal coordinate system. The closed and open circles represent the Lagrangian point on the wall and the probe point near the wall, respectively. The origin o and the point W on the wall coincide with each other.

current work, \vec{u}_w is set to be zero because the flows over a stationary solid body are investigated. Notice that the velocity component u_ζ is zero because the axis $o-\xi$ is defined to be parallel to the tangential velocity near the wall. In the numerical simulation, we need to compute only the tangential velocity at the probe point P as shown in Fig. 1.

The Reynolds-averaged TBL equation for the velocity in the wall-tangential direction is employed to model the flow near the wall (hereinafter referred to as the wall-modeled region),

$$\frac{\partial}{\partial \eta} \left[(v + \nu_t) \frac{\partial \vec{u}}{\partial \eta} \cdot \vec{e}_\xi \right] = S, \tag{11}$$

where $S = \frac{1}{\rho} \nabla \cdot \vec{P} \cdot \vec{e}_\xi + \frac{\partial \vec{u}}{\partial t} \cdot \vec{e}_\xi + (\vec{u} \cdot \nabla) \vec{u} \cdot \vec{e}_\xi$ is the combination of the pressure gradient, local acceleration, and convection terms, ν_t is the eddy viscosity in the wall-modeled region, and \vec{P} is the Reynolds-averaged pressure near the wall.

We integrate Eq. (11) along the wall-normal direction to a probe point P near the wall (as shown in Fig. 1),

$$(v + \nu_t) \frac{\partial u_{\xi,P}}{\partial \eta} = \frac{\tau_w}{\rho} + \int_0^{\delta_p} S d\eta, \tag{12}$$

where $u_{\xi,P}$ is the velocity component along the $o-\xi$ direction at the probe point P , δ_p is the distance from the probe point P to the wall, and τ_w is the wall shear stress. Notice that the integral over S on the right-hand side of Eq. (12) is not directly numerically computed along the line from the wall to the probe point P , since we have not embedded a fine grid to fully resolve the near wall velocities in the current work. Instead, we approximately estimated this term by considering only the pressure gradient term according to the work of Wang and Moin.¹⁰ The details of the approximation, derivation, and implementation will be reported in Subsection III B.

We then construct the virtual slip velocity on the wall by retaining the formally linear distribution of the velocity within the wall-modeled region and adjust the eddy viscosity near the wall to

preserve the momentum balance. Thus, the velocity gradient at the probe point P can be approximated as

$$\frac{\partial u_{\xi,P}}{\partial \eta} = \frac{u_{\xi,P} - u_{\xi,W}}{\delta_P}, \tag{13}$$

where $u_{\xi,W}$ is the slip velocity on the wall at point W . A combination of Eqs. (12) and (13) gives an explicit expression for the slip velocity at point W ,

$$u_{\xi,W} = u_{\xi,P} - \frac{\delta_P}{(v + \nu_t)} \left(\frac{\tau_w}{\rho} + \int_0^{\delta_P} S d\eta \right). \tag{14}$$

Equation (14) is the non-equilibrium slip wall model proposed in this work. For a given point W on the wall, the slip velocity can be computed based on the flow at the probe point P and the wall shear stress τ_w . The probe point P is generally not coincident with the Eulerian grid point. We interpolate the flow variables from the Eulerian grid to the point P by using the MLS method according to the work of Vanella *et al.*⁵⁵ In the current work, the distance between the probe point P and the wall, δ_P , is set as $2.0\Delta h$, where Δh is the grid length of the Eulerian grid. The MSL interpolation stencil points are specified as all grid points located within $1.2\Delta h$ from the probe point P . Thus, no point inside the body is involved in the MLS reconstruction, and the undesired effects associated with cross wall interpolation can be avoided, as shown in Fig. 2(a). The shear stress is computed by using a wall model consistent with Eq. (11), as discussed in Sec. III B.

When the grid resolution is fine enough to resolve the viscous sublayer near the wall, the eddy viscosity and the source term on the

right-hand side of Eq. (14) diminish. In this situation, the slip wall model reduces to the no-slip boundary condition

$$\begin{aligned} u_{\xi,W} &= u_{\xi,P} - \frac{\delta_P}{\nu} \frac{\tau_w}{\rho} \\ &= u_{\xi,P} - \frac{\delta_P}{\nu} \frac{1}{\rho} \left(\mu \frac{u_{\xi,P}}{\delta_P} \right) \\ &= 0. \end{aligned} \tag{15}$$

We use the impenetrable boundary condition¹⁰ as follows for the flows with stationary boundaries:

$$u_{\eta,W} = 0, \tag{16}$$

where $u_{\eta,W}$ is the velocity component in the wall-normal direction at point W .

B. Computation of the wall shear stress

We investigate a simplified variant of the model with $S = 1/\rho(\nabla \bar{P} \cdot \vec{e}_\xi)$ as the non-equilibrium model proposed by Wang and Moin,¹⁰ which accounts for effects of pressure gradient on near wall flows (hereinafter referred to as the NEB model). In this case, Eq. (11) reduces to an ordinary differential equation as follows:

$$\frac{\partial}{\partial \eta} \left[(v + \nu_t) \frac{\partial \bar{u}_\xi}{\partial \eta} \right] = \frac{1}{\rho} \frac{\partial \bar{P}}{\partial \xi}, \tag{17}$$

where $u_\xi = \vec{u} \cdot \vec{e}_\xi$ is the tangential component of velocity, and $\frac{\partial \bar{P}}{\partial \xi} = \nabla \bar{P} \cdot \vec{e}_\xi$ is the pressure gradient along the tangential direction.

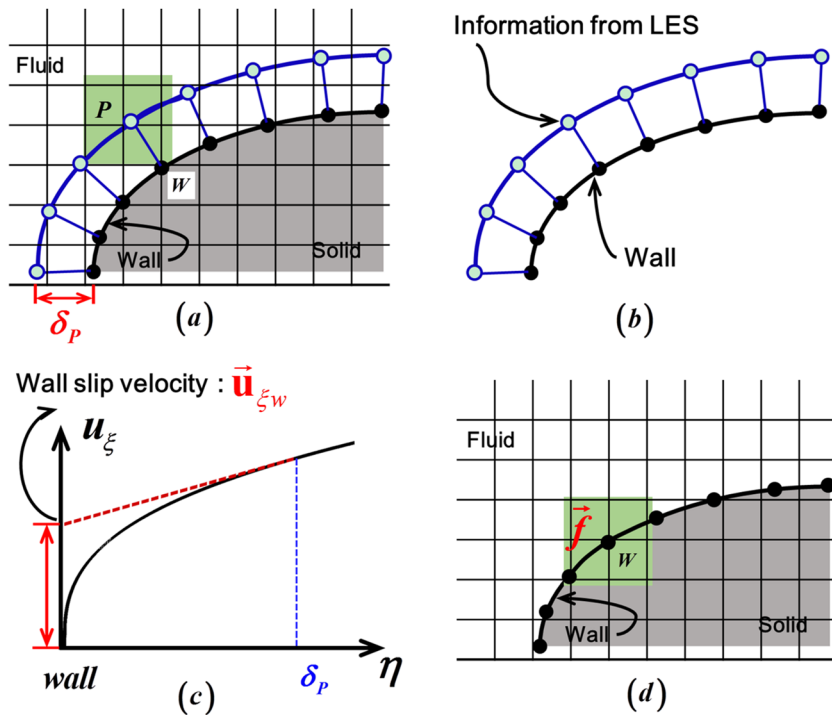


FIG. 2. Schematic illustration of the construction and implementation of the proposed slip wall model. (a) The probe points (open circles, blue online) near the wall and the schematic of the interpolation stencil (square around the point P , green online), (b) the local Lagrangian mesh to compute the wall shear stress, (c) reconstruct the slip velocity on the wall from the wall shear stress by retaining a linear velocity profile near the wall, (d) the body force is computed at the wall using a direct-forcing method using the slip velocity. The black curved lines in (a), (b), and (d) represent the immersed boundary, which is discretized with Lagrangian points (solid black circles). The probe points (open circles, blue online) can be constructed by extruding the Lagrangian points in the normal direction to the wall at a specified distance δ_P . The shaded squares around points represent the interpolation region for the MLS reconstruction.

The integral of Eq. (17) from a point W on the wall to η along the wall-normal direction gives

$$(v + v_t) \frac{\partial u_\xi}{\partial \eta}(\eta) - \tau_w = \int_0^\eta \frac{1}{\rho} \frac{\partial \bar{P}}{\partial \xi} d\eta', \quad (18)$$

where $\tau_w = (v + v_t) \frac{\partial u_\xi}{\partial \eta} \Big|_w = v \frac{\partial u_\xi}{\partial \eta} \Big|_w$ is the wall shear stress at the point W on the wall. η' on the right-hand side of Eq. (18) is an auxiliary variable to distinguish the boundary of the integration η along the wall-normal direction and the independent variable of the pressure gradient $\frac{\partial \bar{P}}{\partial \xi}(\eta')$ along the wall-normal direction.

We introduce the assumption that the pressure gradient along the wall-normal direction is zero within the boundary layer. Based on this assumption, $\frac{1}{\rho} \frac{\partial \bar{P}}{\partial \xi}$ is constant and Eq. (18) reduces to

$$\frac{\partial u_\xi}{\partial \eta}(\eta) = \frac{\tau_w}{v + v_t} + \frac{1}{\rho} \frac{\partial \bar{P}}{\partial \xi} \eta \frac{1}{v + v_t}. \quad (19)$$

We integral Eq. (19) along the wall-normal direction from the wall to the probe point P and obtain the expression in the form of tangential velocity as follows:

$$u_\xi(\eta) = \tau_w \int_0^{\delta_p} \frac{1}{v + v_t} d\eta + \frac{1}{\rho} \frac{\partial \bar{P}}{\partial \xi} \int_0^{\delta_p} \frac{\eta}{v + v_t} d\eta. \quad (20)$$

The rearrangement of Eq. (20) gives the wall shear stress as follows:

$$\tau_w = \frac{\rho}{\int_0^{\delta_p} \frac{d\eta}{v + v_t}} \left\{ u_{\xi,P} - S \int_0^{\delta_p} \frac{\eta d\eta}{v + v_t} \right\}. \quad (21)$$

Here, $u_{\xi,P} = u_\xi(\delta_p)$ is the tangential velocity at the probe point P , and $S = \frac{1}{\rho} \frac{\partial \bar{P}}{\partial \xi}$ is the pressure gradient near wall.

In numerical implementation, we use instantaneous pressure gradient at the probe point P to approximate the term S in Eq. (21),

$$S \approx \frac{1}{\rho} \frac{\partial \bar{p}}{\partial \xi}(\delta p). \quad (22)$$

The eddy viscosity v_t is computed as follows to account for the effect of the pressure gradient:⁵⁸

$$\frac{v_t}{v} = \kappa \eta^* \left[\alpha + \eta^* (1 - \alpha)^{3/2} \right]^\beta \left(1 - e^{-\eta^*/(1+\alpha^3 A)} \right)^2, \quad (23)$$

where $\eta^* = \eta u_{\tau p} / \nu$ is the corrected frictional length, and $u_{\tau p} = \sqrt{u_\tau^2 + u_p^2}$ is a combination of the frictional velocity $u_\tau = \sqrt{|\tau_w|/\rho}$ and the reference velocity defined by the pressure gradient $u_p = |(v/\rho)(\partial \bar{P}_m / \partial \xi)|^{1/3}$. The parameter $\alpha = u_\tau^2 / u_{\tau p}^2$ quantifies the preponderant effect between the shear stress and pressure gradient. The other parameters are set according to those used by Duprat *et al.*,⁵⁸ i.e., $\kappa = 0.41$, $\beta = 0.78$, and $A = 18$. When the pressure gradient is negligible, Eq. (23) reduces to the van Driest formula, which effectively predicts the velocity profile for boundary layers with a zero pressure gradient.

To compute η^* and the wall-layer eddy viscosity v_t in Eq. (23), the friction velocity u_τ is required. In the present implementation,

$u_\tau = \sqrt{|\tau_w|/\rho}$ is evaluated using the instantaneous τ_w from the previous time step according to the work of Wang and Moin.¹⁰ In this sense, the proposed non-equilibrium wall model given by Eq. (14) and the wall shear stress given by Eq. (21) are algebraic. The wall shear stress and the slip velocity on the wall can be calculated by the numerical integration through the boundary condition provided by the probe points in each time step.

To investigate the performance of the non-equilibrium wall model, we also construct another simplified version of Eq. (14) with $S = 0$, which yields an equilibrium wall model (hereinafter referred to as the EB model) as follows:

$$u_{\xi,W} = u_{\xi,P} - \frac{\delta_p}{(v + v_t)} \frac{\tau_w}{\rho}. \quad (24)$$

The performances of the NEB model and the EB model will be discussed in Sec. IV.

C. Implementation of the slip wall model in the framework of immersed boundary method

We implement the slip wall model in the form of a direct-forcing IB method proposed by Vanella and Balaras,⁵⁴ where the body forcing in the momentum equations is computed based on the MLS reconstruction near the wall. This method can be applied to arbitrary moving/deforming bodies with great effectiveness and robustness.⁵⁴

The body forcing, $f_i^{n+1/2}$ in Eq. (6) at the Eulerian grid point (r, s, t) can be calculated as follows:

$$f_i^{n+1/2}(r, s, t) = \sum_L w(r, s, t, L) F_i^{n+1/2}(L), \quad L \in \mathcal{L}, \quad (25)$$

where $F_i^{n+1/2}(L)$ is body forcing at the L th Lagrangian grid point, \mathcal{L} is the set of Lagrangian grid points associated with the considered Eulerian node at (r, s, t) , and $w(r, s, t, L)$ is a weighted function computed by using the MLS method when interpolating the forces from the L th Lagrangian grid point to the Eulerian grid point (r, s, t) . The body forcing on the L th Lagrangian grid point is computed by

$$F_i^{n+1/2}(L) = \frac{U_i^b(L) - \tilde{U}_i^{**}(L)}{\Delta t}, \quad (26)$$

where U_i^b is the slip velocity computed by using Eq. (14) on the L th Lagrangian grid point; \tilde{U}_i^{**} is the predicted velocity at the L th Lagrangian point, which can be interpolated from the surrounding Eulerian grids as follows:

$$\tilde{U}_i^{**}(L) = \sum_{(r,s,t) \in \mathcal{E}} w(L, r, s, t) \hat{u}_i^{**}, \quad (r, s, t) \in \mathcal{E}, \quad (27)$$

where \mathcal{E} is the set of the Eulerian grid points associated with the L th Lagrangian marker, and \hat{u}_i^{**} is the predicted velocity in the Eulerian grids and can be computed using Eq. (6) without the body force $f_i^{n+1/2}$, i.e.,

$$\hat{u}_i^{**} = \tilde{u}^n + \Delta t \left(rhs^{n+1/2} - \frac{\partial \bar{p}^n}{\partial x_i} \right). \quad (28)$$

The procedures of constructing and implementing the proposed slip wall model are summarized as follows:

- (i) Interpolate the flows from the Eulerian mesh to the probe points, as shown in Fig. 2(a).
- (ii) Compute the wall shear stress based on the flow on the probe points according to Eq. (21), as shown in Fig. 2(b).
- (iii) Construct the slip velocity on the wall based on the wall shear stress and the flow at the probe points according to Eq. (14), as shown in Fig. 2(c).
- (iv) Compute the body forcing for the IB method according to Eq. (25), as shown in Fig. 2(d).

IV. RESULTS AND DISCUSSION

This work combines the non-equilibrium wall model with the IB method. The new development is that we propose to implement the wall model as a slip wall boundary condition in the framework of IB method. The features of the proposed model are (i) feeding the LES with slip velocity boundary condition, instead of the wall shear stress boundary condition; (ii) accounting for the non-equilibrium effect associated with the pressure gradient. The validations used in this section are designed with the focuses on the validity of the new development. The wall-modeled LES of plane channel turbulence is conducted to validate the first feature of the proposed model, i.e., the application of the slip velocity boundary condition instead of wall shear stress boundary condition. The flows over a backward-facing step are simulated to validate the capability of the proposed model in handling flows with pressure gradient near the wall. We would like to note that the Reynolds number in the flows over the backward facing step is relatively low, although it is one of the most widely used cases in validating the wall modeled LES in the literature. However, there is no well-documented benchmark at high Reynolds numbers. To avoid the fairly fine resolution of the grid in this case, we conducted the wall-modeled LES on a very coarse grid, which is comparable to the widely used grid lengths in validating the wall-models reported in the literature.

A. Plane channel turbulence

The errors of the current wall-modeled LES depend on the errors of modeling the near wall flow and the errors of constructing and implementing the slip velocity. The plane channel turbulence is an appropriate case for investigating the validity of constructing and implementing the slip velocity because Eq. (11) gives a good modeling of the near wall flow in plane channels. Plane channel turbulence is an extensively investigated wall-bounded flow and it serves as a benchmark to validate the wall-modeled LES. We use the equilibrium wall model, $S = 0$ in Eq. (14), for the plane channel turbulence. The validity of Eq. (11) for plane channel turbulence can be clearly seen in the *a priori* test shown in Fig. 3, where Eq. (11) with $S = 0$ is integrated along the wall-normal direction

$$u_{\xi}(\eta) = \frac{\tau_w}{\rho} \int_0^{\eta} \frac{d\eta'}{\nu + \nu_t}. \quad (29)$$

For given wall shear stresses at $Re_{\tau} = 1000, 2000,$ and 5200 , the mean velocity profiles near the wall predicted by Eq. (29) agree well with those of direct numerical simulation (DNS) given by Lee and Moser,⁵⁹ where Re_{τ} is computed based on the friction velocity u_{τ} , the channel half height h , and the kinematic viscosity ν .

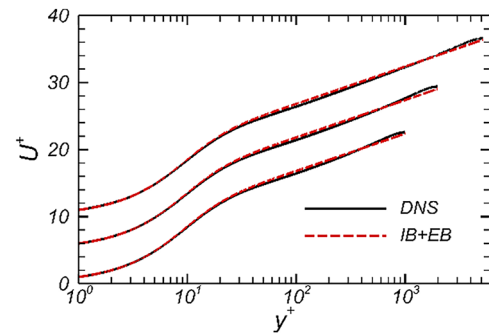


FIG. 3. Comparison of the mean velocity profiles of turbulent channel flow at $Re_{\tau} = 1000, 2000,$ and 5200 (from the bottom up) in the *a priori* test. The profiles are shifted up by four units for clarity of visualization.

Besides the *a priori* test, the validity of constructing and implementing the slip velocity are investigated by the *a posteriori* test at $Re_{\tau} = 2000$, where the LES is conducted with the EB model. The computational domain is a rectangular domain of $8\pi h \times 3h \times \pi h$ in the streamwise, wall-normal, and spanwise directions, respectively, as shown in Fig. 4(a). We discretize the computational domain using uniform Eulerian grids. The channel walls are immersed in the computational domain and discretized as uniform Lagrangian grid with the same grid length as the Eulerian grid. The Lagrangian grid points are intentionally positioned to be not coincident with the Eulerian grid points, to mimic the relative position of the Eulerian grid points and Lagrangian grid points for a general shape, as shown in Fig. 4(b). The proposed slip wall model with $S = 0$ in Eq. (14) is implemented on the wall by using the IB method. The periodic boundary conditions are applied on the computational domain in the streamwise and spanwise directions. The flow is initially evolved up to a non-dimensional time of $30h/u_{\tau}$ with a constant mass flux, and statistics are obtained for an additional $10h/u_{\tau}$ non-dimensional time.

We conduct the simulations on two different grids with $\Delta h = h/32$ ($\Delta h^+ = 125$) and $\Delta h = h/16$ ($\Delta h^+ = 250$), respectively. The mean streamwise velocity profiles are plotted against the wall distance using the inner and outer scales, respectively, as shown in Fig. 5. Both the simulations give the acceptable mean streamwise velocity profiles outside the probe point. The velocity profile on the coarse mesh ($\Delta h^+ = 250$) slightly deviates from the DNS result. This is caused by the large distance between the probe point P and the wall, $\delta p^+ = 2\Delta h^+ = 500$, where the probe point P is in the margin of the logarithmic layer. The deviation is notably suppressed on the fine mesh with $\Delta h^+ = 125$ ($\Delta h = h/32$), where the probe point is within the logarithmic layer, as shown in Fig. 5(b).

Figure 6 shows the distributions of the Reynolds stresses across the channel in the simulation on the grid with $\Delta h^+ = 125$ ($\Delta h = h/32$). The predictions to the Reynolds stress far from the wall ($y/h > 0.3$) are acceptable, although the predictions in the near wall region deviates from the DNS results. The proposed model overpredicts the streamwise velocity fluctuations and underpredicts the normal and spanwise velocity fluctuations, which is a persistent problem in the wall-modeled LES.⁵⁰ The similar results of overpredictions and underpredictions to the velocity fluctuations are also reported in the wall-modeled LES on the boundary conformal mesh

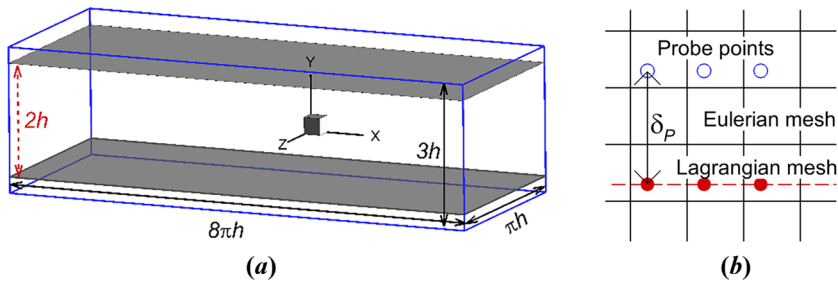


FIG. 4. Schematics of (a) the computational domain of the channel flow and (b) the Eulerian and Lagrangian meshes. The Lagrangian mesh nodes are intentionally positioned to be not coincident with the Eulerian mesh nodes.

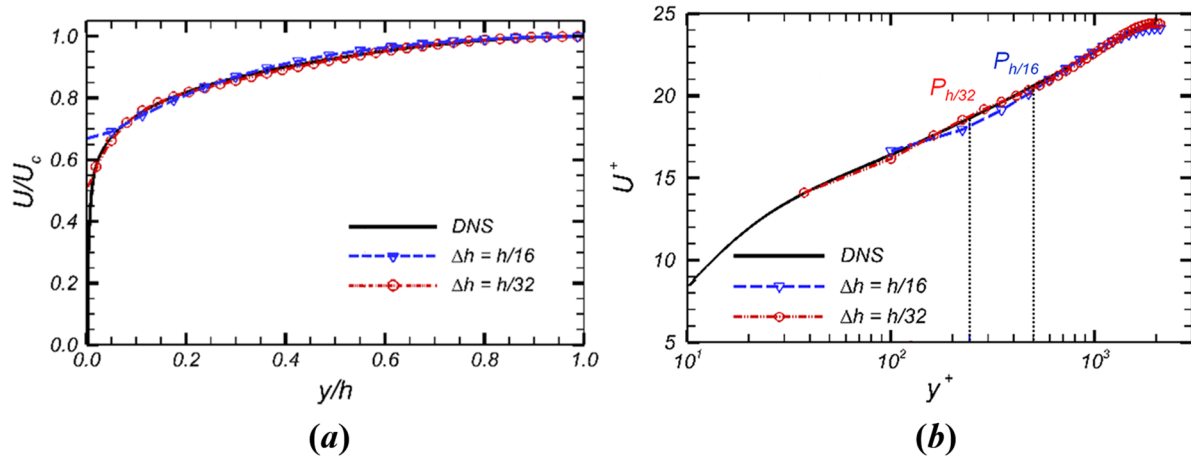


FIG. 5. Mean velocity profiles of the turbulent channel flow at $Re_\tau = 2000$ in (a) outer scales and (b) inner scales. U_c is the channel center velocity, and $P_{h/16}$ and $P_{h/32}$ indicate the positions of the probe points in the simulations with coarse and fine meshes, respectively. The solid lines represent the DNS data of Lee and Moser.⁵⁹

method.^{58,60,61} Wang *et al.*⁶¹ comprehensively assessed the capability of different wall models in predicting the turbulence kinetic energy. They find that the wall models can reasonably predict the turbulence fluctuations far from the wall, although the near-wall flows are not fully resolved. It is of great challenge to improve the velocity fluctuations near the wall for wall-modeled LES.⁵¹ Since we focus on proposing a way to accounting for the non-equilibrium effect in the

framework of the IB method in the current work, we have not tuned the proposed model with special treatments near the wall to improve the prediction of velocity fluctuations. The audiences can refer to the recent models^{50,62–64} with specific handling of the flow details in the vicinity of the wall for improving the predictions of velocity fluctuations.

The LES of plane channel turbulence with the proposed model shows that it is valid to construct and implement the wall model in the form of slip velocity on the wall. The proposed model gives a fairly good prediction of the mean velocity profiles. The prediction of the Reynolds stresses is acceptable in the region far from the walls ($y/h > 0.3$). The discrepancy of the velocity fluctuations near the wall is a persistent problem, since the grid length in wall-modeled LES is much larger than wall units ($\Delta h^+ = 125$ in the current work). The results given by the proposed model are consistent with those of wall-modeled LES on boundary conformal mesh method.

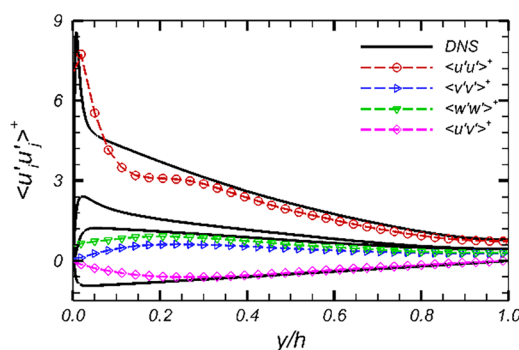


FIG. 6. Distribution of the resolved part of the Reynolds stresses in the turbulent channel flow on the fine-grid region with $\Delta h = h/32$. From top to bottom, $\langle u'u' \rangle$, $\langle v'v' \rangle$, $\langle w'w' \rangle$, and $\langle u'v' \rangle$. The solid lines are the DNS data of Lee and Moser.⁵⁹

B. Backward-facing step flow

The flow over a backward-facing step in a channel is a benchmark test case for the non-equilibrium wall models. The flow subjects to a sudden change of cross section, which results in a separation at the end edge of the backward-facing step and forms a separation bubble with non-neglectable pressure gradient behind the step. We conduct the wall-modeled LES using the proposed slip wall model with both the NEB model and the EB model.

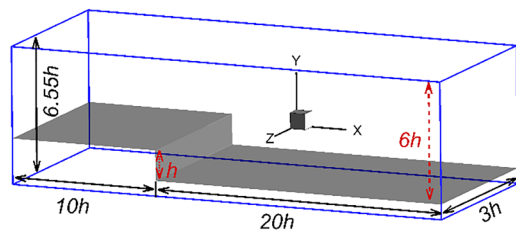


FIG. 7. Schematic illustration of the backward-facing step flow configuration and definition of the computational domain.

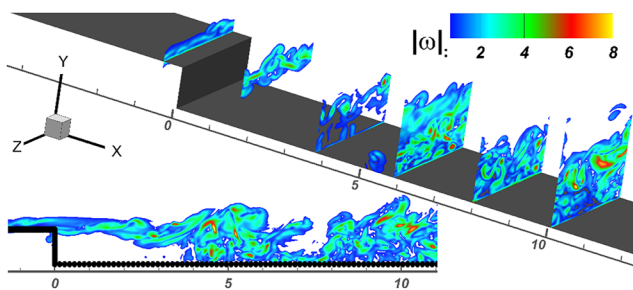


FIG. 8. Instantaneous flow structures characterized by the distribution of the vorticity magnitude from different points of view (predicted by the NEB model).

The channel with the backward-facing step has an expansion ratio of 1.2. The Reynolds number in the simulations is $Re_h = U_0 h / \nu = 5000$, where U_0 is the maximum inlet velocity, and the h is the step height. The results are compared with the experimental study by Jovic and Driver⁶⁵ at the same Reynolds number and the DNS analysis conducted by Le *et al.*⁶⁶ at $Re_h = U_0 h / \nu = 5100$ based on a body-conformal mesh.

The simulation is conducted in a rectangular domain of $30h \times 6.55h \times 3h$ in the streamwise, normal, and spanwise directions, respectively, as shown in Fig. 7. The backward-facing step is immersed in the rectangular domain with a distance of $10h$ from the inlet to the step surface. The velocity profile at the inlet is a flat-plate turbulent boundary layer profile,⁶⁷ and the boundary layer thickness is $\delta_{99} = 1.2h$. A free-convection boundary condition is set at

the outlet, periodic boundary condition is applied in the spanwise directions, and free-slip boundary condition is used on the top and bottom boundary of the computational domain. The slip-velocity on the immersed step (the gray surface in Fig. 7) is constructed by using the proposed model and implemented in the form of the IB method. The flow is initialized with flat-plate boundary velocity in the region of $h \leq y \leq 6.55h$ and zero within the region of $0 \leq y < h$. The flow is developed for 20 “flow through” times, and the statistics are taken for an additional 15 “flow through” times.

We discretized the computational domain by using an Eulerian uniform grid with a grid length of $\Delta h = h/16$. The immersed backward-facing step is discretized by using a uniform Lagrangian grid with the same grid length as the Eulerian grid. The Lagrangian grid points are intentionally positioned to not coincide with the Eulerian grid points as that in the case of the plane channel turbulence.

Figure 8 shows the instantaneous vorticity magnitude, where the boundary layer sheds from the step and forms the shear layer in the near wake. The vorticity in the shear layer interacts with the mean velocity and the wall, resulting in complex flow structures in the downstream. The flow reattaches to the wall and forms a recirculation region. Both the NEB model and EB model give a correct prediction of the average reattachment length of about $6.3h$ according to the zero wall shear stress, as shown in Fig. 9(a). The skin-friction and surface pressure coefficients predicted by using the proposed model are consistent with those reported in the wall-modeled LES on a boundary conformal mesh. The EB model severely underpredicts the skin-friction coefficient in the recirculation region, as shown in Fig. 9(a). The skin-friction coefficient predicted by using the EB model is less than one half of the DNS result or the experimental measurements within the recirculation region. The underprediction is similar to that reported in the work of Cabot and Moin,⁶⁰ in which the LES is conducted with different wall models on boundary conformal meshes and the underprediction is found to be related to the equilibrium flow assumption near the wall.

The skin-friction is reported to be sensitive to the pressure gradient.⁶⁸ The NEB model accounting for the effects of pressure gradient on the near wall gives acceptable results in the recirculation region, as shown in Fig. 9(a). The NEB model overpredicts the skin friction after the reattachment. The overprediction of the skin friction coefficient near the exit is also reported in the work of Cabot and

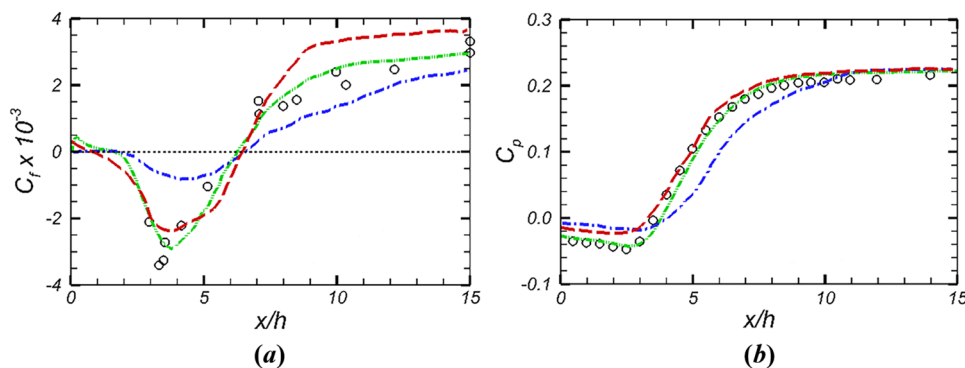


FIG. 9. Distribution of the time-averaged (a) skin-friction and (b) surface pressure coefficients on the bottom surface in the backward-facing step flow. The experimental results of Jovic and Driver⁶⁵ (open circles) and the direct numerical simulation results of Le *et al.*⁶⁶ (the green dashed-dotted lines) are taken as references. The blue dashed-dotted lines and red dashed lines are the results predicted by the EB and NEB slip wall models, respectively. The dotted line in (a) indicates the line of $C_f = 0$.

Moin⁶⁰ when the non-equilibrium TBL equation model is used on a boundary conformal mesh and the overprediction is considered to be related to the rapid change of the velocity near the wall for a fixed free stream in a channel.

The pressure coefficient on the bottom wall drops immediately after the step and recovers gradually after the reattachment point, as shown in Fig. 9(b). The EB model severely underpredicts the pressure drop around the recirculation region with high pressure gradient ($x/h < 7.0$), while the NEB model greatly improves the prediction by accounting for the non-equilibrium associated with the pressure gradient.

The velocity profiles behind the step are shown in Fig. 10. The NEB model gives a better prediction of the mean velocity profiles in the recirculation region than the EB model, although both of them give a fairly good prediction of the mean velocity profiles behind the reattachment point, as shown in Fig. 10(a). This is because the effects of pressure gradient cannot be ignored in the recirculation region and is ignorable in the attached flow region. The EB model without accounting for the pressure gradient gives a large deviation of the mean velocity profiles in the wall-modeled region, as shown in Fig. 11. The mean velocity profiles in Fig. 11 reflect the validity of the way to model the near wall flows. The mean velocity profiles for the EB model is computed by using Eq. (29) where the effects of the pressure gradient are ignored. The mean velocity profiles for the NEB model are computed by

$$u_\xi(\eta) = \frac{\tau_w}{\rho} \int_0^\eta \frac{d\eta'}{v + v_t} + \int_0^\eta \int_0^\eta \left(\frac{1}{\rho} \frac{\partial p}{\partial \xi} \right)_w d\eta' d\eta', \quad (30)$$

where $\left(\frac{\partial p}{\partial \xi} \right)_w$ is the tangential pressure gradient on the wall. The EB model cannot correctly give the mean velocity profiles in the recirculation region. The NEB model improves the results remarkably although only the non-equilibrium effect associated with the pressure gradient is taken into account. The deficiencies are expected to

be associated with the neglected convection terms.⁶⁸ The NEB model also gives a fairly good prediction of the velocity fluctuations and the Reynolds stress, while those predicted by using the EB model have relatively large discrepancies, as shown in Figs. 10(b)–10(d).

The results show that the proposed non-equilibrium wall model is able to give an acceptable prediction of the wall stresses and the flow statistics on a coarse grid. Compared to the equilibrium model, the inclusion of the non-equilibrium effect associated with the pressure gradient in the NEB model gives a remarkable improvement of the results.

We would like to note that the validations in this section are designed to validate the proposed way to implement the non-equilibrium wall model in the IB method as a slip-wall boundary condition. We just use a simple non-equilibrium wall model, where the effects of pressure gradients on the wall shear stress are taken into account while the effects of the convective terms are discarded. Larsson *et al.*²¹ show that the discarding of the convective terms might result in inconsistencies because the pressure gradient is essentially balanced by the convection outside of the viscous layer. The accounting for the convective terms might improve the velocity profiles near the wall.^{21,68,69} The non-equilibrium effects associated with the unsteady and convection terms can be taken into account in the way similar to the pressure gradient. Another way to improve the near wall flow statistics is to use a transpiration velocity instead of the no-transpiration velocity in the wall-normal direction. The slip velocity in the wall-parallel direction with the transpiration velocity in the wall-normal direction are reported to improve the prediction of turbulence intensities by avoiding the formation of long streaks and relaxing the blocking effect of the wall.⁵⁰ However, it is not trivial to correctly model all the statistics behaviors of the non-equilibrium near wall flows on a coarse mesh. Efforts should be paid to tune the way to couple the wall models with the flows at the probe points and the way to compute the near wall eddy viscosity, which are expected to be investigated in future work.

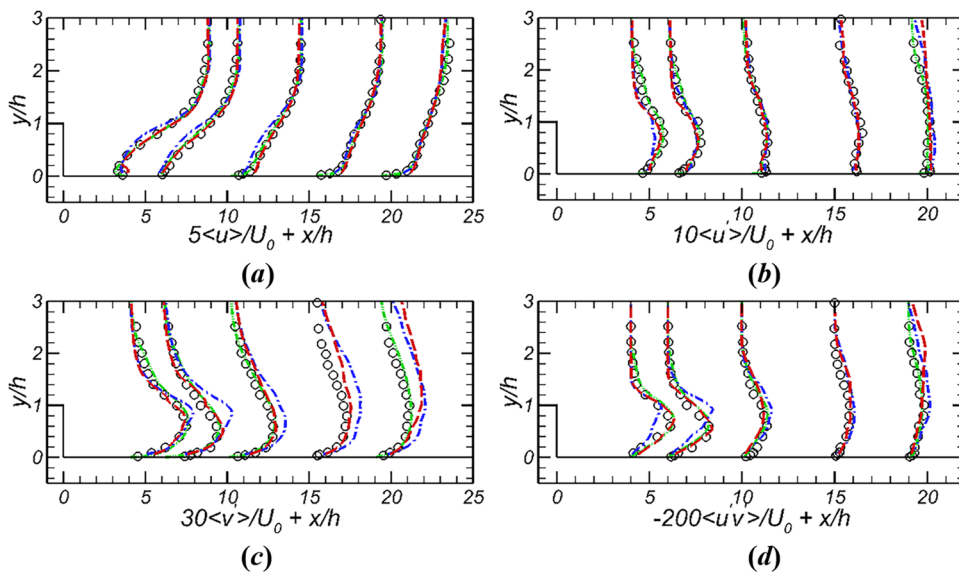


FIG. 10. Velocity profiles of the (a) mean streamwise velocity, (b) RMS of the streamwise velocity fluctuations, (c) RMS of the normal velocity fluctuations, and (d) the Reynolds shear stress profiles for backward-facing step flow at five downstream stations ($x/h = 4.0, 6.0, 10.0, 15.0,$ and 19.0 from left to right). The experimental results of Jovic and Driver⁶⁵ (open circles) and the direct numerical simulation results of Le *et al.*⁶⁶ (the green dashed-dotted lines) are taken as references. The blue dashed-dotted lines and red dashed lines are the results predicted by the EB and NEB slip wall models, respectively.

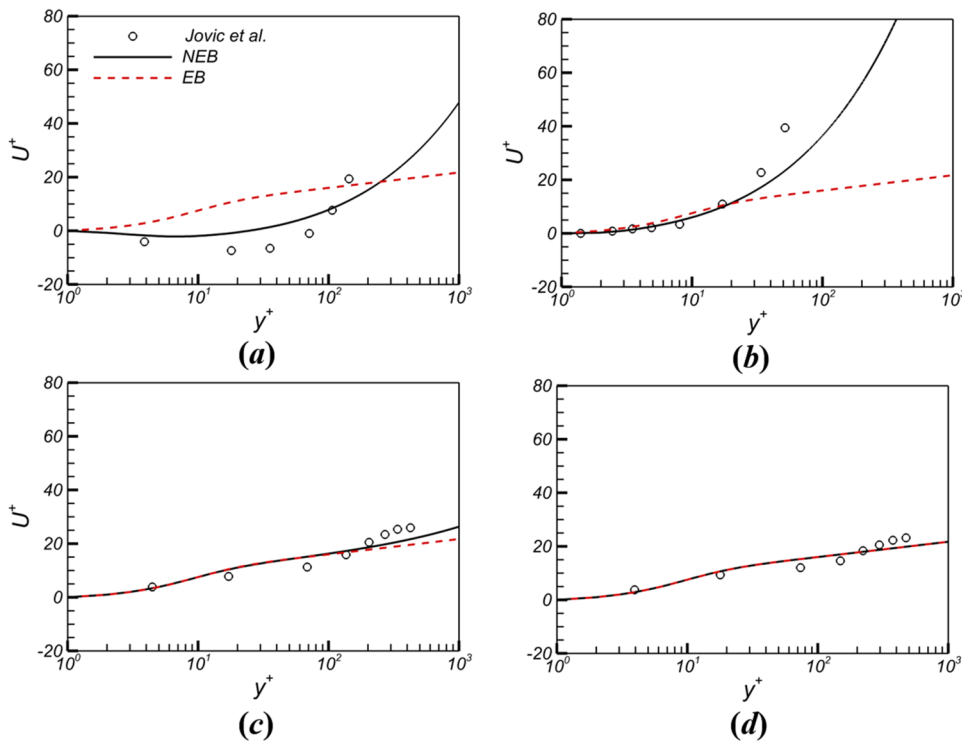


FIG. 11. Distributions of the mean streamwise velocity of the flow over a backward-facing step at (a) $x/h = 4.0$, (b) $x/h = 6.0$, (c) $x/h = 10.0$, and (d) $x/h = 15.0$.

V. SUMMARY AND CONCLUSIONS

The combination of the wall model with the IB method provides a feasible approach for LES of turbulent flows with non-canonical boundaries at a reasonable computational cost. We proposed a slip wall model for LES with the IB method to account for the non-equilibrium flow near the wall. The proposed wall model feeds the LES with a slip velocity on the wall. The slip velocity is constructed based on the integral of the simplified thin boundary layer equation near the wall to improve the momentum balance on a coarse grid. The non-equilibrium flow associated with the pressure gradient is taken into account by retaining the pressure gradient term in the simplified thin boundary layer equation. The proposed slip wall model is implemented in the framework of direct-forcing IB method with MLS reconstructions near the wall.

We validated the proposed model by the wall-modeled LES of plane channel turbulence and the flows over a backward-facing step. Both the velocity profiles and the wall stresses were consistent with the experimental or numerical results. Compared to the equilibrium wall model for LES with the IB method, the proposed non-equilibrium wall model greatly improved the numerical results on relatively coarse grids. In particular, the equilibrium wall model underpredicts the wall shear stress and deviates from the correct velocity fluctuations in the recirculation region in the flow over the backward-facing step, while the proposed non-equilibrium wall model considerably improved the predictions. The results show that the proposed slip wall model is a feasible approach to account for the non-equilibrium flow near the wall in LES with the IB method.

ACKNOWLEDGMENTS

This work was supported by the NSFC Basic Science Center Program for “Multiscale Problems in Nonlinear Mechanics” (Grant No. 11988102) and the National Natural Science Foundation of China (Grant No. 11922214). The computations are conducted on Tianhe-1 at the National Supercomputer Center in Tianjin.

AUTHOR DECLARATIONS

Conflict of Interest

The authors have no conflicts to disclose.

Author Contributions

Beiji Shi and Zhaoyue Xu contributed equally to this work.

Beiji Shi: Data curation (equal); Validation (equal); Visualization (equal); Writing – original draft (equal). **Zhaoyue Xu:** Data curation (equal); Validation (equal); Visualization (equal). **Shizhao Wang:** Conceptualization (equal); Methodology (equal); Supervision (equal); Writing – original draft (equal); Writing – review & editing (equal).

DATA AVAILABILITY

The data that support the findings of this study are available from the corresponding author upon reasonable request.

REFERENCES

- ¹U. Piomelli and E. Balaras, "Wall-layer models for large-eddy simulations," *Annu. Rev. Fluid Mech.* **34**, 349–374 (2002).
- ²S. T. Bose and G. I. Park, "Wall-modeled large-eddy simulation for complex turbulent flows," *Annu. Rev. Fluid Mech.* **50**, 535–561 (2018).
- ³X. Zheng and G. Wang, "Progresses and challenges of high Reynolds number wall-bounded turbulence," *Adv. Mech.* **50**, 202001 (2020).
- ⁴W. Kim and H. Choi, "Immersed boundary methods for fluid-structure interaction: A review," *Int. J. Heat Fluid Flow* **75**, 301–309 (2019).
- ⁵W. Huang and F. Tian, "Recent trends and progresses in the immersed boundary method," *Proc. Inst. Mech. Eng., Part C: Journal of Mechanical Engineering Science* **233**, 7617 (2019).
- ⁶A. Posa and E. Balaras, "Model-based near-wall reconstructions for immersed-boundary methods," *Theor. Comput. Fluid Dyn.* **28**, 473–483 (2014).
- ⁷A. Cristallo and R. Verzicco, "Combined immersed boundary/large-eddy-simulations of incompressible three dimensional complex flows," *Flow, Turbul. Combust.* **77**, 3–26 (2006).
- ⁸G. Iaccarino and R. Verzicco, "Immersed boundary technique for turbulent flow simulations," *Appl. Mech. Rev.* **56**, 331–347 (2003).
- ⁹U. Schumann, "Subgrid scale model for finite difference simulations of turbulent flows in plane channels and annuli," *J. Comput. Phys.* **18**, 376–404 (1975).
- ¹⁰M. Wang and P. Moin, "Dynamic wall modeling for large-eddy simulation of complex turbulent flows," *Phys. Fluids* **14**, 2043–2051 (2002).
- ¹¹H. Werner and H. Wengle, "Large-eddy simulation of turbulent flow over and around a cube in a plate channel," in *Turbulent Shear Flows 8*, edited by F. Durst, R. Friedrich, B. E. Launder, F. W. Schmidt, U. Schumann, and J. H. Whitelaw (Springer, Berlin, Heidelberg, 1993), pp. 155–168.
- ¹²U. Piomelli, J. Ferziger, P. Moin, and J. Kim, "New approximate boundary conditions for large eddy simulations of wall-bounded flows," *Phys. Fluids A* **1**, 1061–1068 (1989).
- ¹³M. Breuer and W. Rodi, "Large eddy simulation for complex turbulent flows of practical interest," in *Flow Simulation with High-Performance Computers II*, Notes on Numerical Fluid Mechanics (NNFM), edited by E. H. Hirschel (Vieweg, 1996), Vol. 48, pp. 258–274.
- ¹⁴G. John-Puthenveetil and S. Jakirlic, "On 'adaptive wall-functions' for LES of flow and heat transfer," in *New Results in Numerical and Experimental Fluid Mechanics IX*, Notes on Numerical Fluid Mechanics and Multidisciplinary Design, edited by A. Dillmann, G. Heller, E. Krämer, H.-P. Kreplin, W. Nitsche, and U. Rist (Springer International Publishing, Cham, 2014), Vol. 124, pp. 103–112.
- ¹⁵E. Balaras, C. Benocci, and U. Piomelli, "Two-layer approximate boundary conditions for large-eddy simulations," *AIAA J.* **34**, 1111–1119 (1996).
- ¹⁶X. I. A. Yang, J. Sadique, R. Mittal, and C. Meneveau, "Integral wall model for large eddy simulations of wall-bounded turbulent flows," *Phys. Fluids* **27**, 025112 (2015).
- ¹⁷K. Suga, T. Sakamoto, and Y. Kuwata, "Algebraic non-equilibrium wall-stress modeling for large eddy simulation based on analytical integration of the thin boundary-layer equation," *Phys. Fluids* **31**, 075109 (2019).
- ¹⁸S.-G. Cai and P. Sagaut, "Explicit wall models for large eddy simulation," *Phys. Fluids* **33**, 041703 (2021).
- ¹⁹H. Hosseinzade and D. J. Bergstrom, "Time-averaging and temporal-filtering in wall-modeled large eddy simulation," *Phys. Fluids* **33**, 035108 (2021).
- ²⁰H.-N. Wang, W.-X. Huang, and C.-X. Xu, "Synthetic near-wall small-scale turbulence and its application in wall-modeled large-eddy simulation," *Phys. Fluids* **33**, 095102 (2021).
- ²¹J. Larsson, S. Kawai, J. Bodart, and I. Bermejo-Moreno, "Large eddy simulation with modeled wall-stress: Recent progress and future directions," *Mech. Eng. Rev.* **3**, 1500418 (2016).
- ²²K. Nakahashi, "Aeronautical CFD in the age of petaflops-scale computing: From unstructured to Cartesian meshes," *Eur. J. Mech. B* **40**, 75–86 (2013).
- ²³H. Park, G. Oh, T. S. Park, C. Lee, and J.-I. Choi, "An immersed boundary formulation incorporating a two-layer wall model approach for rans simulations with complex geometry," *Comput. Fluids* **205**, 104551 (2020).
- ²⁴Y. Tamaki and S. Kawai, "Wall modeling for large-eddy simulation on non-body-conforming Cartesian grids," *Phys. Rev. Fluids* **6**, 114603 (2021).
- ²⁵I. Cheylan, J. Favier, and P. Sagaut, "Immersed boundary conditions for moving objects in turbulent flows with the lattice-Boltzmann method," *Phys. Fluids* **33**, 095101 (2021).
- ²⁶X. Xue, H.-D. Yao, and L. Davidson, "Synthetic turbulence generator for lattice Boltzmann method at the interface between RANS and LES," *Phys. Fluids* **34**, 055118 (2022).
- ²⁷B. Tian, J. Chen, X. Zhao, M. Zhang, and B. Huang, "Numerical analysis of interaction between turbulent structures and transient sheet/cloud cavitation," *Phys. Fluids* **34**, 047116 (2022).
- ²⁸F. Roman, V. Armenio, and J. Fröhlich, "A simple wall-layer model for large eddy simulation with immersed boundary method," *Phys. Fluids* **21**, 101701 (2009).
- ²⁹H. Asmuth, C. F. Janßen, H. Olivares-Espinosa, and S. Ivanell, "Wall-modeled lattice Boltzmann large-eddy simulation of neutral atmospheric boundary layers," *Phys. Fluids* **33**, 105111 (2021).
- ³⁰C. S. Peskin, "Flow patterns around heart valves: A numerical method," *J. Comput. Phys.* **10**, 252–271 (1972).
- ³¹C. S. Peskin, "The immersed boundary method," *Acta Numer.* **11**, 479–517 (2002).
- ³²F. Sotiropoulos and X. Yang, "Immersed boundary methods for simulating fluid–structure interaction," *Prog. Aerosp. Sci.* **65**, 1–21 (2014).
- ³³S.-J. Li, J.-H. Pan, and M.-J. Ni, "A fast mapping method to evaluate immersed boundary hydrodynamic forces," *Acta Mech. Sin.* **38**, 721491 (2022).
- ³⁴Z. Zhou, Z. Li, G. He, and X. Yang, "Towards multi-fidelity simulation of flows around an underwater vehicle with appendages and propeller," *Theor. Appl. Mech. Lett.* **12**, 100318 (2022).
- ³⁵S. Li, X. Yang, G. Jin, and G. He, "Wall-resolved large-eddy simulation of turbulent channel flows with rough walls," *Theor. Appl. Mech. Lett.* **11**, 100228 (2021).
- ³⁶D. Li, A. Wei, K. Luo, and J. Fan, "An improved moving-least-squares reconstruction for immersed boundary method," *Int. J. Numer. Methods Eng.* **104**, 789–804 (2015).
- ³⁷Z. A. Wei and Z. C. Zheng, "Energy-harvesting mechanism of a heaving airfoil in a vortical wake," *AIAA J.* **55**, 4061–4073 (2017).
- ³⁸Y. D. Jeong and J. H. Lee, "Passive control of a single flexible flag using two side-by-side flags," *Int. J. Heat Fluid Flow* **65**, 90–104 (2017).
- ³⁹J. Ryu, S. G. Park, and H. J. Sung, "Flapping dynamics of inverted flags in a side-by-side arrangement," *Int. J. Heat Fluid Flow* **70**, 131–140 (2018).
- ⁴⁰G. Liu, Y. Ren, H. Dong, O. Akanyeti, J. C. Liao, and G. V. Lauder, "Computational analysis of vortex dynamics and performance enhancement due to body–fin and fin–fin interactions in fish-like locomotion," *J. Fluid Mech.* **829**, 65–88 (2017).
- ⁴¹B. Kim, S. G. Park, W.-X. Huang, and H. J. Sung, "An autonomous flexible propulsor in a quiescent flow," *Int. J. Heat Fluid Flow* **68**, 151–157 (2017).
- ⁴²C. Yan, W.-X. Huang, G.-X. Cui, C. Xu, and Z.-S. Zhang, "A ghost-cell immersed boundary method for large eddy simulation of flows in complex geometries," *Int. J. Comput. Fluid Dyn.* **29**, 12–25 (2015).
- ⁴³A. Posa, M. Vanella, and E. Balaras, "An adaptive reconstruction for Lagrangian, direct-forcing, immersed-boundary methods," *J. Comput. Phys.* **351**, 422–436 (2017).
- ⁴⁴B. Kye, K. Park, H. Choi, M. Lee, and J.-H. Kim, "Flow characteristics in a volute-type centrifugal pump using large eddy simulation," *Int. J. Heat Fluid Flow* **72**, 52–60 (2018).
- ⁴⁵M. Ma, W.-X. Huang, C.-X. Xu, and G.-X. Cui, "A hybrid immersed boundary/wall-model approach for large-eddy simulation of high-Reynolds-number turbulent flows," *Int. J. Heat Fluid Flow* **88**, 108769 (2021).
- ⁴⁶R. Mittal and G. Iaccarino, "Immersed boundary methods," *Annu. Rev. Fluid Mech.* **37**, 239–261 (2005).
- ⁴⁷E. Balaras, "Modeling complex boundaries using an external force field on fixed Cartesian grids in large-eddy simulations," *Comput. Fluids* **33**, 375–404 (2004).
- ⁴⁸F. Tessicini, G. Iaccarino, M. Fatica, M. Wang, and R. Verzicco, "Wall modeling for large-eddy simulation using an immersed boundary method," *Tech. Rep.*, Center for Turbulence Research, 2002.

- ⁴⁹J.-I. Choi, R. C. Oberoi, J. R. Edwards, and J. A. Rosati, "An immersed boundary method for complex incompressible flows," *J. Comput. Phys.* **224**, 757–784 (2007).
- ⁵⁰H. J. Bae, A. Lozano-Durán, S. T. Bose, and P. Moin, "Turbulence intensities in large-eddy simulation of wall-bounded flows," *Phys. Rev. Fluids* **3**, 014610 (2018).
- ⁵¹H. J. Bae, A. Lozano-Durán, S. T. Bose, and P. Moin, "Dynamic slip wall model for large-eddy simulation," *J. Fluid Mech.* **859**, 400–432 (2019).
- ⁵²X. Yang and S. Bose, "A physical basis of the slip-wall model for wall-modeled large-eddy simulations," 10th International Symposium on Turbulence and Shear Flow Phenomena, TSFP10, 2017.
- ⁵³F. Nicoud and F. Ducros, "Subgrid-scale stress modelling based on the square of the velocity gradient tensor," *Flow, Turbul. Combust.* **62**, 183–200 (1999).
- ⁵⁴M. Vanella and E. Balaras, "A moving-least-squares reconstruction for embedded-boundary formulations," *J. Comput. Phys.* **228**, 6617–6628 (2009).
- ⁵⁵M. Vanella, S. Wang, and E. Balaras, "Direct and large-eddy simulations of biological flows," in *Direct and Large-Eddy Simulation X*, edited by D. G. Grigoriadis, B. J. Geurts, H. Kuerten, J. Fröhlich, and V. Armenio (Springer International Publishing, 2018), pp. 43–51.
- ⁵⁶S. Wang, M. Vanella, and E. Balaras, "A hydrodynamic stress model for simulating turbulence/particle interactions with immersed boundary methods," *J. Comput. Phys.* **382**, 240–263 (2019).
- ⁵⁷B. Shi, X. Yang, G. Jin, G. He, and S. Wang, "Wall-modeling for large-eddy simulation of flows around an axisymmetric body using the diffuse-interface immersed boundary method," *Appl. Math. Mech.* **40**, 305–320 (2019).
- ⁵⁸C. Duprat, G. Balarac, O. Métais, P. M. Congedo, and O. Brugière, "A wall-layer model for large-eddy simulations of turbulent flows with/out pressure gradient," *Phys. Fluids* **23**, 015101 (2011).
- ⁵⁹M. Lee and R. D. Moser, "Direct numerical simulation of turbulent channel flow up to $Re_\tau \approx 5200$," *J. Fluid Mech.* **774**, 395–415 (2015).
- ⁶⁰W. Cabot and P. Moin, "Approximate wall boundary conditions in the large-eddy simulation of high Reynolds number flow," *Flow, Turbul. Combust.* **63**, 269–291 (2000).
- ⁶¹L. Wang, R. Hu, and X. Zheng, "A comparative study on the large-scale-resolving capability of wall-modeled large-eddy simulation," *Phys. Fluids* **32**, 035102 (2020).
- ⁶²A. Keating and U. Piomelli, "A dynamic stochastic forcing method as a wall-layer model for large-eddy simulation," *J. Turbul.* **7**, N12 (2006).
- ⁶³L. Davidson and M. Billson, "Hybrid LES-RANS using synthesized turbulent fluctuations for forcing in the interface region," *Int. J. Heat Fluid Flow* **27**, 1028–1042 (2006).
- ⁶⁴S. Blanchard, N. Odier, L. Gicquel, B. Cuenot, and F. Nicoud, "Stochastic forcing for sub-grid scale models in wall-modeled large-eddy simulation," *Phys. Fluids* **33**, 095123 (2021).
- ⁶⁵S. Jovic and D. Driver, "Backward-facing step measurements at low Reynolds number, $Re_h = 5000$," NASA Technical Memorandum 108807, 1994.
- ⁶⁶H. Le, P. Moin, and J. Kim, "Direct numerical simulation of turbulent flow over a backward-facing step," *J. Fluid Mech.* **330**, 349–374 (1997).
- ⁶⁷P. R. Spalart, "Direct simulation of a turbulent boundary layer up to $Re_\theta = 1410$," *J. Fluid Mech.* **187**, 61–98 (1988).
- ⁶⁸Z. Chen, S. Hickel, A. Devesa, J. Berland, and N. A. Adams, "Wall modeling for implicit large-eddy simulation and immersed-interface methods," *Theor. Comput. Fluid Dyn.* **28**, 1–21 (2014).
- ⁶⁹A. Frere, K. Hillewaert, P. Chatelain, and G. Winckelmans, "High Reynolds number airfoil: From wall-resolved to wall-modeled LES," *Flow, Turbul. Combust.* **101**, 457–476 (2018).